Minimum-aperture Kirchhoff migration using CRS attributes

C. Jäger

email: *Christoph.Jaeger@gpi.uka.de*

keywords: *Kirchhoff migration, CRS attributes, minimum aperture, stationary point, true amplitudes*

ABSTRACT

The efficiency of Kirchhoff migration as well as the achievable image quality depend strongly on the selection of the migration aperture. The use of small apertures speeds up migration with the drawback that steeply dipping reflectors cannot be imaged properly. By choosing larger apertures, steep reflectors, e. g. the flanks of salt domes, can be imaged. But as a consequence, run time increases and the steep migration operators can cause operator aliasing which has to be suppressed by suitable anti-alias filters. These filters slow down the migration even more and, often, make a true-amplitude processing impossible. The kinematic wavefield attributes that are determined in a data-driven way by means of the Common-Reflection-Surface stack allow to compute a minimum migration aperture independently for each point in the migration target zone. The application of minimum-aperture Kirchhoff pre- and poststack migration to a complex synthetic data set as well as to real data demonstrates that this technique is able to produce images of hight quality with increased computational efficiency.

INTRODUCTION

In recent years, many case studies have demonstrated that the data-driven Common-Reflection-Surface (CRS) stack (e.g. Müller, 1999; Jäger et al., 2001; Mann, 2002) produces reliable stack sections with an excellent signal-to-noise (S/N) ratio. In addition, an entire set of physically interpretable stacking parameters, so-called kinematic wavefield or CRS attributes, is determined. This additional information is very useful in further processing: Duveneck (2004) shows how the attributes can be used for the determination of a velocity model by means of an attribute-based tomographic inversion which has several advantages compared to conventional velocity inversion tools. Furthermore, properties like, e. g., the geometrical spreading factor (Vieth, 2001) or the projected Fresnel zone (Vieth, 2001; Mann, 2002) can be estimated by means of the kinematic wavefield attributes. The attributes can also be utilized for residual static corrections (Koglin and Ewig, 2003). Pruessmann et al. (2004) demonstrate that even AVO analysis can benefit from the CRS approach. In this paper, I will show how the CRS attributes can be used to improve efficiency and image quality of Kirchhoff migration.

Kirchhoff migration is a flexible, target-oriented, efficient, and, thus, frequently applied migration technique. Kirchhoff depth migration treats each point on a sufficiently dense grid in the subsurface as a potential diffraction point. The migration output that is assigned to such a depth point M is obtained by stacking the amplitudes of the filtered input seismogram along its configuration-specific diffraction traveltime curve (2D migration) or surface (3D migration). If desired, the effect of geometrical spreading can be removed from the output amplitudes by multiplying the data during the stack with a true-amplitude weight function. Then, the amplitudes in the obtained migration result can serve as a measure of the angle-dependent reflection coefficient provided that other influences on the amplitude such as, e. g., transmission loss or source/receiver coupling effects are modest or can be corrected for. As can be seen from Figure 1, it is sufficient to restrict the migration operator to that part lying within the reflection signal strip around the stationary point ξ^* at which the migration operator and the reflection event have the same slope. Summing only input amplitudes within this *minimum aperture* increases the computational efficiency, enhances

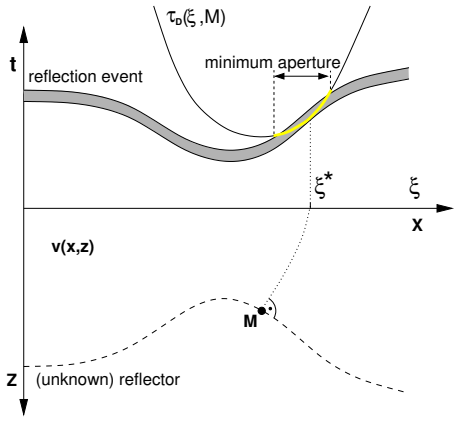

Figure 1: Principle of Kirchhoff migration. The migration result for a depth point M is obtained by summing the amplitudes of the input seismogram along the diffraction traveltime curve/surface $\tau_D(\xi, M)$ of the considered subsurface point. The minimum aperture is depicted in yellow.

image quality especially in the presence of noise, and reduces boundary effects (Schleicher et al., 1997). Unfortunately, the stationary point is in practice not known prior to migration. Therefore, the aperture is usually limited by a user-defined maximum dip or aperture radius. In the following section, I will show how the attributes of the 2D zero-offset (ZO) CRS stack can serve for the determination of this ideal aperture for 2D Kirchhoff depth migration.

DETERMINATION OF THE MINIMUM APERTURE

The determination of the minimum aperture for Kirchhoff migration consists of two tasks: (1) the determination of the stationary point for the considered output grid point M and (2) the computation of the horizontal extent of the minimum aperture around the previously determined stationary point.

Poststack migration

One of the three attributes that are determined for every ZO time sample (ξ, t_0) by means of the 2D ZO CRS stack (in the following simply called CRS stack) is the emergence angle $\alpha = \alpha(\xi, t_0)$ of the ZO normal ray. The midpoint coordinate of an input trace is denoted by ξ, t_0 is the two-way traveltime. As can be seen from Figure 2, α is directly related to the slope β of events in the stacked ZO section by

$$\tan\beta = \frac{2}{v_0}\sin\alpha\,, \tag{1}$$

where v_0 is the near-surface velocity that was used in the previously applied CRS stack. The stationary point ξ^* is the midpoint location at which the migration operator for the considered depth point M is tangent to an actual event in the input time section. Therefore, at the stationary point ξ^*

$$\beta(\xi, \tau_D(\xi, M)) - \beta_{\text{op}}(\xi) = 0\big|_{\xi=\xi^*}\,, \tag{2}$$

where $\tau_D(\xi, M)$ is the migration operator (=diffraction traveltime curve) for point M and $\beta_{\text{op}}(\xi)$ is the dip of this operator at location ξ. Since β_{op} can be easily determined from the traveltime tables that are computed prior to migration and β can be readily obtained from the CRS attribute α using equation (1), all information necessary for the determination of the stationary point by means of equation (2) are available.

Once the stationary point has been computed, the radius of the minimum aperture must be determined. Schleicher et al. (1997) have shown that the horizontal extent of this optimum migration aperture is in paraxial approximation equivalent to the radius of the projected Fresnel zone (PFZ) of a wave with frequency $\omega = 2\pi/\tau_L$ where τ_L is a measure of the pulse length of the source signal. The radius of the PFZ

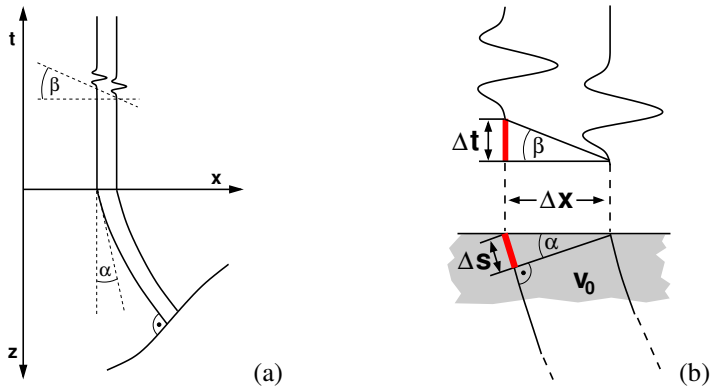

Figure 2: The emergence angle α of a ZO normal ray is directly related to the local slope β of the associated event in the ZO time section via the near-surface velocity v_0.

for the ZO configuration can be approximated with CRS attributes as (Vieth, 2001; Mann, 2002)

$$r_{\text{pfz}} = |\xi - \xi_0| = \frac{1}{\cos\alpha}\sqrt{\frac{v_0\tau_L}{2\left|\frac{1}{R_{\text{NIP}}} - \frac{1}{R_{\text{N}}}\right|}}, \tag{3}$$

with R_{NIP} and R_{N} being the radius of the NIP and normal wave, respectively. For an explanation of the CRS attributes see, e. g., Jäger et al. (2001). With this equation, the radius of the minimum aperture can be computed at the previously detected stationary points.

The CRS attributes do not only allow the computation of the minimum aperture for Kirchhoff migration; also the true-amplitude weight function for Kirchhoff poststack migration (e. g. Hanitzsch, 1997) can be expressed purely in terms of CRS attributes (Vieth, 2001).

The strategy for minimum-aperture poststack Kirchhoff migration that has to be performed for all points M in the migration target zone can be summarized as follows:

1. Computation of the stacking operator $\tau_D(\xi, M)$ and its slope $\beta_{\text{op}}(\xi)$ for all ξ.

2. Computation of the difference between the operator dip and the dip of reflection events encountered along the operator in the ZO section $\Delta(\xi) = |\beta(\xi, \tau_D(M, \xi)) - \beta_{\text{op}}(\xi)|$ for all ξ along the operator.

3. Determination of the minimum of $\Delta(\xi)$. If this minimum is smaller than a user-defined threshold, it is assumed to be located at the stationary point ξ^* and step 4 is executed. If not, the current subsurface point M is not located on an actual reflector, no summation has to be performed, and we continue with step 1 for the next point M in the target zone.

4. Computation of the radius of the PFZ by means of equation (3) and summation of all amplitudes encountered along the stacking operator in the range $|\xi - \xi^*| \leq r_{\text{pfz}}$ to obtain the migration result $V(M)$. If desired, a true-amplitude weight function calculated from the CRS attributes (or, e. g., from dynamic ray tracing) can be applied at this step.

Parameters that have to be specified by the user are (1) a threshold value for the maximum allowed difference $|\beta - \beta_{\text{op}}|$ at a stationary point, (2) a measure of the wavelet length τ_L and (3) a coherence threshold above which CRS attributes are assumed to be reliable. Stationary points (ξ^*, t_0) associated with a coherency below this threshold are rejected.

In an optional output file, all points M having a stationary point are stored together with their respective location ξ^* and the associated radius of the PFZ for zero offset. This information is necessary for a subsequent prestack migration with minimum aperture.

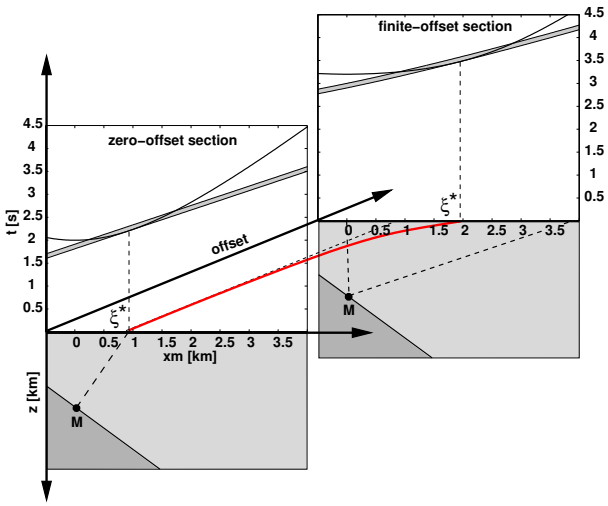

Figure 3: The CRP trajectory (red curve) consists of all source(S)-receiver(R) combinations (described by midpoint and offset coordinate) for which the rays SMR (dashed) describe specular reflections in a common depth point M. The offset-dependency of the stationary point ξ^* pertaining to the depicted depth point M is given by its associated CRP trajectory. In two selected common-offset time sections the reflection event (shaded) of the dipping interface is shown together with the diffraction traveltime curve of M. They are tangent to each other at the stationary point $\xi^*(h)$.

Prestack migration

Seismic data are usually acquired in such a way that subsurface points on reflecting interfaces are illuminated by several source-receiver pairs with different offset. The common-reflection-point (CRP) trajectory is that curve in the time-midpoint-offset volume along which all information pertaining to one subsurface reflection point is gathered. In the following, however, I will refer to the CRP trajectory as the projection of this spherical curve onto the midpoint-offset plane (Figure 3). For prestack migration with minimum aperture of such multi-coverage data sets, we must know the location of the stationary point ξ^* and the radius of the PFZ r_{pfz} for all (half-)offsets h contained in the input data. Unfortunately, it is not possible to determine $\xi^*(h)$ and $r_{\text{pfz}}(h)$ directly from the attributes of the ZO CRS stack. Nevertheless, the offset-dependency of the location of the stationary point ξ^* can be determined from the CRP trajectory once $\xi^*(h=0)$ is known for the considered M as is illustrated in Figure 3. The CRP trajectory can be approximately expressed by CRS parameters as (Höcht et al., 1999)

$$x_{\text{m}}(h) = x_0 + r_{\text{T}}\left(\sqrt{\frac{h^2}{r_{\text{T}}^2}+1}-1\right) \quad \text{with} \quad r_{\text{T}} = \frac{R_{\text{NIP}}}{2\sin\alpha}\,. \tag{4}$$

The center of the minimum aperture for prestack migration can therefore be calculated for any offset from the CRS attributes and the result of the poststack migration.

The width of the PFZ increases for reasonable depth models with offset. A further quantification of $r_{\text{pfz}}(h)$ is, however, complicated since the PFZ depends on the velocity model and the dip and curvature of the considered reflectors. Therefore, in the current implementation of minimum-aperture prestack migration, the width of the aperture is increased linearly with offset by an user-defined gradient. Of course this approximation is rather brute. But nevertheless, for practical applications the linear estimate of $r_{\text{pfz}}(h)$ turned out to be sufficient. More important than the precise knowledge of the width of the minimum aperture is the fact that the CRP trajectory allows to center this migration aperture at the correct midpoint location, namely at the stationary point $\xi^*(h)$. The variation of the radius of the PFZ with offset for the very simple model of a plane interface beneath a homogeneous overburden is shown in Figure 4. For deeper reflectors the offset dependency of $r_{\text{pfz}}(h)$ decreases.

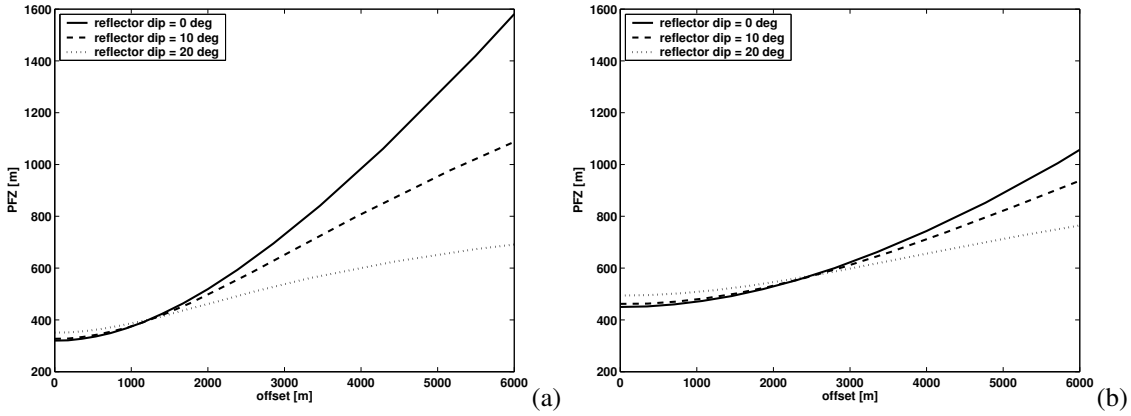

Figure 4: Radius of the PFZ for a plane interface with a dip of $0°$, $10°$, and $20°$ beneath a homogeneous overburden with $v = 2000$ m/s. The reflection point is located at a depth of $z = 1000$ m (a) and $z = 2000$ m (b). The curves are calculated for a source pulse with $\tau_L = 10$ ms.

APPLICATIONS

The presented technique for the determination of the stationary points and the calculation of the minimum aperture radius is implemented (as an option) in the migration program `Uni3D`. In the following sections, this strategy for 2D Kirchhoff depth migration with minimum aperture is demonstrated for a synthetic as well as a real data set and the results are compared with conventional Kirchhoff migration results. Since the same implementation for conventional and minimum-aperture Kirchhoff migration is used, run time and image quality of the different methods may be compared.

Synthetic data example

A synthetic data example is very suitable for testing new migration algorithms because only in this case the obtained results can be compared with their expected, analytically calculated counterparts. Therefore, a synthetic multi-coverage data set was created by ray tracing in the complex 2.5D depth model shown in Figure 5. The prestack data were modeled with a marine acquisition geometry: 576 shots were placed in increments of 20 m, the streamer attached to the left of the vessel consisted of 100 receivers with offsets ranging from 0 m to 1980 m (receiver increment 20 m). The temporal sampling interval was 2 ms. Transmission loss and diffractions due to pinch-outs were not modeled. The resulting ZO section of this data set is displayed in Figure 6a. Although noise was added to the seismogram before CRS stack and migration, this section is shown without noise for a better visualization of the ray tracing artifacts (gaps and amplitude discontinuities along reflectors) that will distort the amplitudes in the migration result. The traveltime table for migration was computed by ray tracing in a smoothed version of the blocky velocity model. In this table, the traveltime is stored on a coarse grid with a shot-, x-, and z-spacing of 50 m, 50 m, and 25 m, respectively. During migration, traveltimes are interpolated linearly onto the desired output grid.

The CRS stack was applied to the multi-coverage data yielding the simulated ZO section Figure 6b together with a set of kinematic wavefield attributes.

Poststack migration Input for the poststack depth migration was the stacked section, Figure 6b. Figure 7a shows all points in the migration target zone for which a stationary point was found by comparing the dip of their diffraction traveltime curve β_{op} with the slope of reflection events β determined from the CRS attribute α. Instead of computing the difference $|\beta - \beta_{\text{op}}|$ for all shot locations of the input seismogram, the search for the stationary points was performed on the coarse shot grid of the traveltime table. This is justified because the migration operator pertaining to an actual reflection point is tangent to the associated reflection event in an extended region rather than at an isolated point. For the stationary points found in this way, the radius of the PFZ is displayed in Figure 7b. Only for depth points associated with a stationary point, the actual migration process is then carried out. The resulting migrated image is shown in

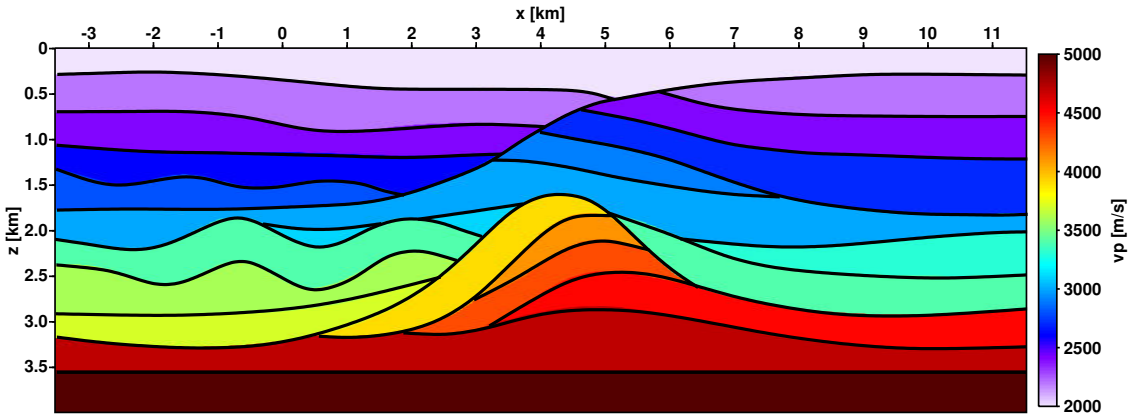

Figure 5: Depth model used for ray tracing. The model consists of homogeneous blocks with P-wave velocities between 2 and 5 km/s.

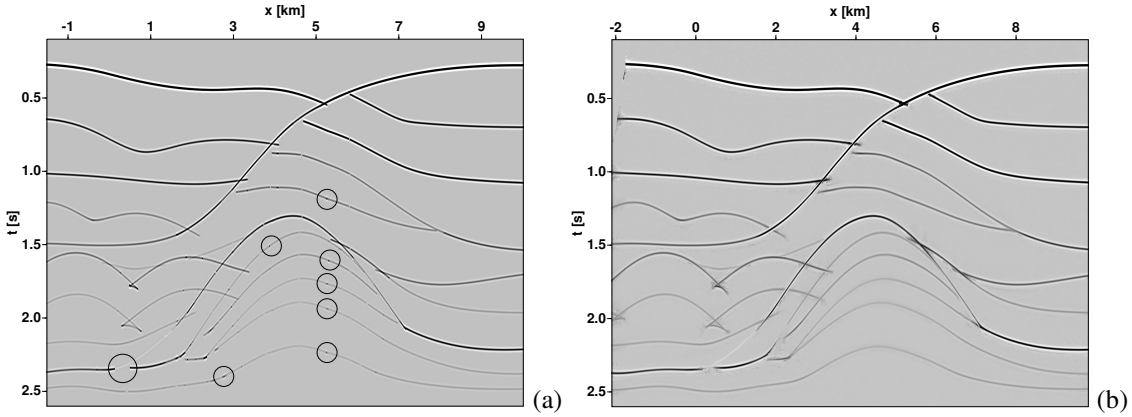

Figure 6: Forward modeled ZO section (a) without noise. Some ray tracing artifacts are marked. Simulated ZO section (b) obtained by means of the CRS stack.

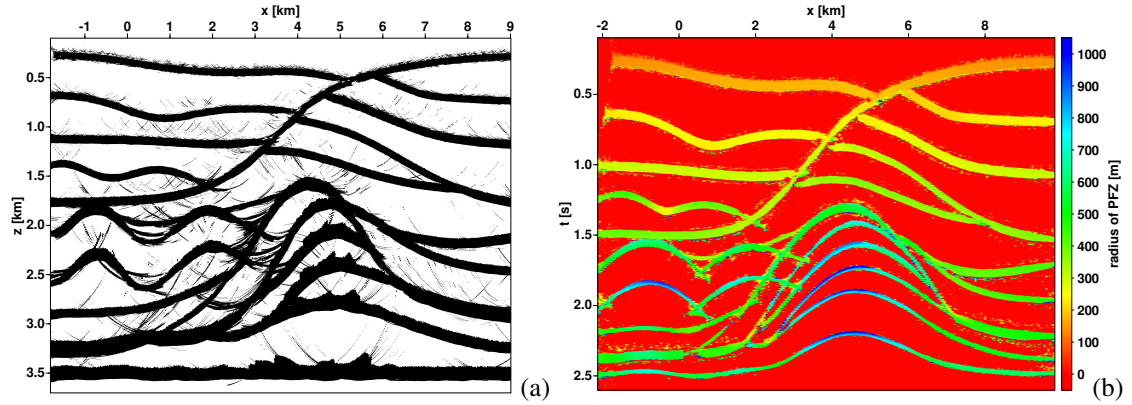

Figure 7: (a) All points in the target zone for which a stationary point has been found (324.000 out of 974.000 target zone grid points). (b) Radius of the PFZ computed from CRS attributes for the stationary points corresponding to the depth points in (a).

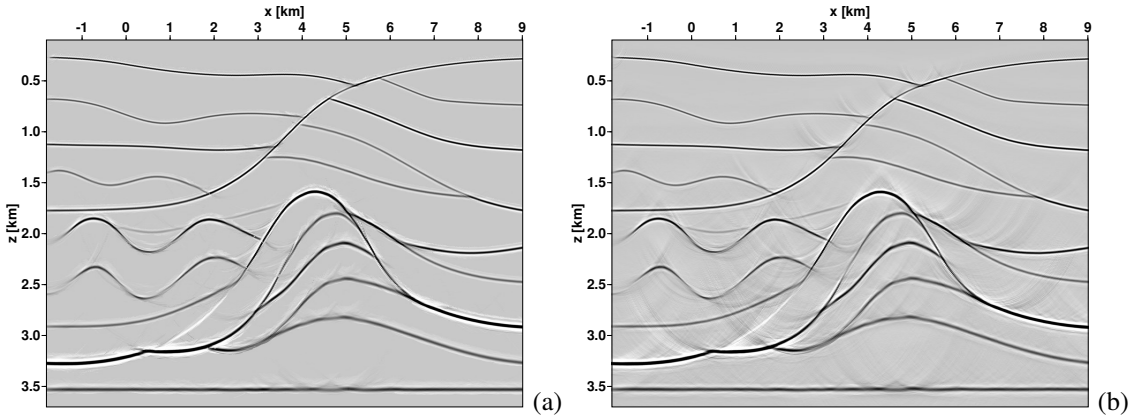

Figure 8: Poststack Kirchhoff migration with minimum aperture determined from CRS attributes (a) and conventional Kirchhoff migration (b) with an aperture increasing linearly with depth.

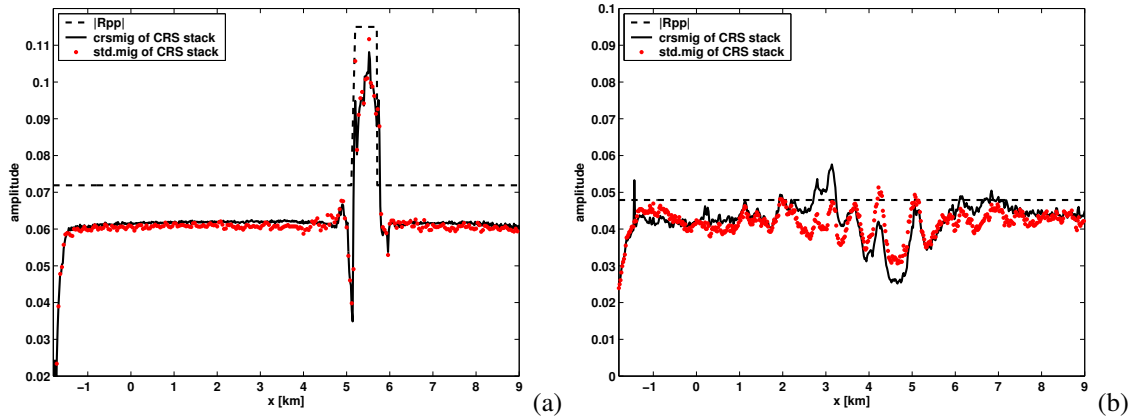

Figure 9: Amplitudes picked along the uppermost (a) and lowermost (b) reflector in the poststack migration result, Figure 8. Dashed black line: normal-incidence reflection coefficient; solid black line: poststack migration of CRS stack result, TA weights computed from CRS attributes; red dots: poststack migration of CRS stack result, TA weights from dynamic ray tracing

Figure 8a. For comparison, Figure 8b depicts the result of a conventional Kirchhoff poststack migration. The conventional migration result contains artifacts due to missing diffractions and amplitude discontinuities along reflectors in the input data. The resulting isochrone-like artifacts are completely suppressed by the proposed migration scheme. As can be seen from Figure 7b, the automatically determined minimum migration aperture only exceeds 500 m for points on top of the anticline structure. Since the stationary points are not known for the conventional Kirchhoff migration, the radius of the migration aperture was chosen to increase linearly from 150 m at the top to 2000 m at the bottom of the target zone. The large aperture is necessary in order to properly image the flanks of the dome-like structure. Despite the additional search for the stationary points, migration with minimum aperture decreased the computation time by 35% compared to conventional Kirchhoff migration.

Amplitudes after true-amplitude post(CRS)stack migration To obtain the migration result shown in Figure 8a, a true-amplitude weight function determined from the CRS attributes was applied during the stack. Since transmission loss was not taken into account in the modeling of the input seismogram and a source with unit strength was used, amplitudes in the true-amplitude-migrated image should be equal to the normal-incidence reflection coefficient. In Figure 9, the amplitudes along the uppermost (a) and lowermost (b) reflector of Figure 8a are depicted (solid black line) together with the analytically calculated

value (dashed black line). For the uppermost interface, the amplitudes picked in the migrated image are about 15% too low but show the same behavior as the reflection coefficient, the jump in the impedance contrast is well recovered. For comparison, the CRS-stacked section was also true-amplitude migrated with conventional Kirchhoff migration where the weight was determined by dynamic ray tracing. The resulting amplitudes (depicted as red dots) match very well to the ones in the migration result, Figure 8a.

The amplitude error of 15% is, therefore, a consequence of the previous stacking process which mixes amplitudes pertaining to different reflection angles (offsets) and CMP locations. While choosing the spatial CRS aperture as large as possible yields stacked sections of very high S/N ratio, smaller CRS apertures are advantageous in order to obtain meaningful amplitudes after poststack migration. But even for data with high S/N ratio, the CRS aperture must not be chosen arbitrarily small: for a stable determination of the CRS attributes R_{NIP} and R_{N} that are associated with second-order traveltime derivatives in midpoint and offset direction, respectively, a sufficiently large aperture is mandatory. A possible solution would be to specify different CRS apertures for the attribute search and the subsequent stacking.

The amplitudes along the lowermost reflector are closer to the theoretical value (average error about 10%) but show much stronger fluctuations. The reason for the smaller over-all error is that a given offset results in the smaller reflection angles the deeper the considered interface is. As a consequence, the offset-dependency of the input amplitude is weaker for deeper reflections and the stacked amplitudes are closer to the zero-offset value. The observed fluctuations are mainly caused by the amplitude discontinuities along reflectors in the input data (see Figure 6a). These ray tracing artifacts are also contained in the stacked section as can be seen from the smiles in Figure 8b. Furthermore, later arrivals are not considered in the migration process which might explain the lower amplitudes below the more complex part of the model in the region between 3 km and 6 km. Due to the complex overburden, reflections from this part are likely to show non-hyperbolic moveout. Therefore, the CRS operator does not fit as well to these reflection events as it does for events located more to the left or right (this can actually be observed by lower values in the coherence section for ZO samples below the dome-like structure). In this region, also the true-amplitude weight function approximated from CRS attributes yields slightly different amplitudes than the weight computed by means of dynamic ray tracing.

Prestack migration After the poststack migration, all depth points M having a stationary point are known together with the location $\xi^*(h = 0)$ of the stationary point and the corresponding radius of the PFZ for the zero-offset configuration. For a prestack migration of the multi-coverage data set, the offset-dependency of ξ^* is calculated from the CRS attributes by means of the CRP trajectory and the migration aperture is increased linearly with offset with a gradient of 3/km. The prestack migration is performed only for points in the target zone for which a stationary point was found by the previous poststack migration (see Figure 7a). The migration result obtained in this way is depicted in Figure 10a, a conventionally prestack-migrated image is displayed in Figure 10b. The respective common-image gathers are shown in Figure 11. Similarly to the poststack migration result, artifacts that are contained in the conventional migration output are very well suppressed by the minium aperture approach. The migration result displayed in Figure 10a was obtained in less than 10% of the computing time of the conventional migration.

Real data example

The reflection seismic data used for the following case study were acquired by an energy resource company. To get a detailed knowledge of the subsurface structure in the area of interest, data were acquired along two parallel lines denoted as A and B. On each line, about 240 geophone groups were laid out in a fixed-spread geometry with a group spacing of 50 m. The source signal was a linear upsweep from 12 Hz to 100 Hz of 10 s duration, generated by three vibrators. The source spacing was 50 m and the temporal sampling interval was 2 ms. For the examples shown in this paper, data from line A are used.

After standard preprocessing of the field data, a stacked ZO section (Figure 12a) was produced by means of the CRS stack. Then, the obtained CRS attributes were utilized in a tomographic inversion scheme to obtain the smooth interval velocity model depicted in Figure 12b. By ray tracing in this model, the traveltime table for migration was created with a shot-, x-, and z-spacing of 50 m, 60 m, and 60 m, respectively.

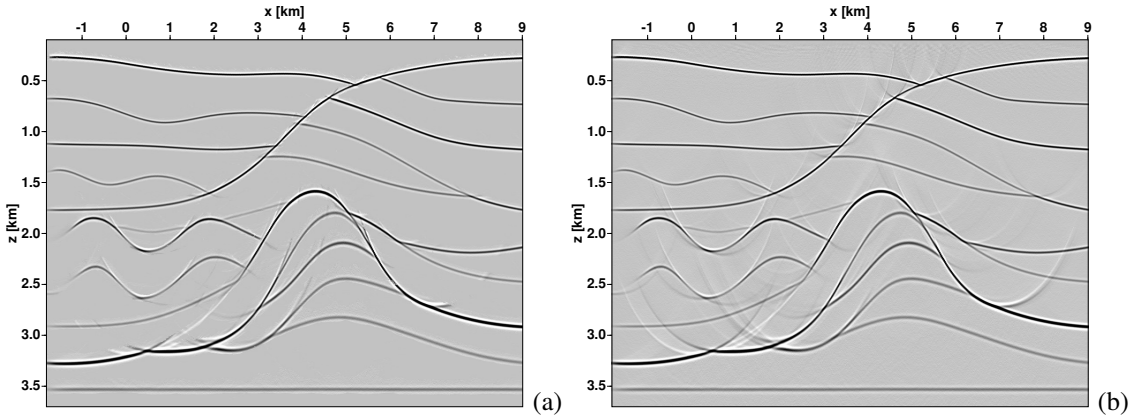

Figure 10: Prestack Kirchhoff migration with minimum aperture determined from CRS attributes (a) and conventional Kirchhoff migration (b) with an aperture increasing linearly with depth. Stack over offsets.

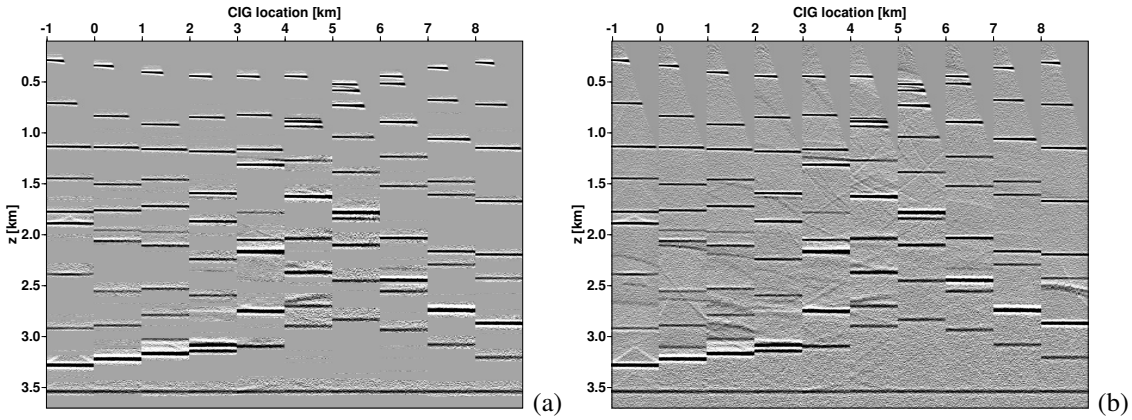

Figure 11: Common-image gathers extracted from the prestack migration results that were used for the stacks shown in Figure 10.

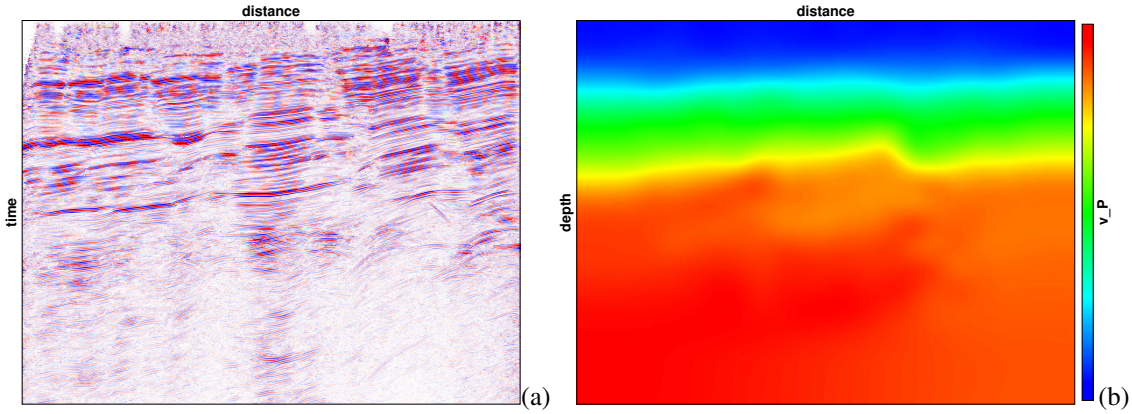

Figure 12: (a) ZO section obtained by means of the CRS stack and (b) velocity model determined from a CRS-attributed-based tomographic inversion.

Poststack migration The depth image after minimum-aperture Kirchhoff migration of the stacked section (Figure 12a) is displayed in Figure 13a. The thresholds for the minimum coherence and the maximum allowed difference $|\beta - \beta_{\text{op}}|$ at a stationary point were chosen such that a stationary point is found for almost every grid point M in the migration target zone (627.000 out of 636.000 grid points in the target zone). In order to quickly get a rough image of the subsurface, only dominant reflectors characterized by high coherence values can be migrated by selecting an appropriate coherence threshold. The result after conventional Kirchhoff migration is shown in Figure 13b. There, large migration apertures had to be chosen to properly image the steeply dipping reflector element marked by an arrow. These large apertures lead to operator aliasing which degraded the migration output. In practice, these aliasing effects are avoided or at least reduced by applying suitable anti-alias filters. This filtering slows down migration and usually influences the amplitudes in the migration output. In the presented example, the runtime was identical for minimum-aperture and conventional Kirchhoff migration. The overhead due to the search for the stationary point was, therefore, compensated by stacking within smaller apertures. Amplitudes are not studied for this real data example since no amplitude-preserving preprocessing had been performed.

Prestack migration By means of a subsequent prestack migration, the subsurface images displayed in Figure 14a (minimum-aperture migration) and 14b (conventional migration) were obtained. The computation time for the minimum-aperture migration was 1/3 of the computation time for the conventional migration. Both results are very similar. However, a steeply dipping event was imaged by the conventional prestack migration (see lower arrow in Figure 14b) which cannot be seen in the minimum-aperture prestack migration result. This event is also not visible in neither of the two poststack-migrated images, Figure 13a and 13b, it is only illuminated by larger offsets. In the current implementation of minimum-aperture migration, stationary points are searched for in the ZO section and are then extrapolated to finite offsets for prestack migration. With this approach, only events that are visible or detectable in the stacked section can be properly imaged by the minimum-aperture prestack migration.

OUTLOOK & CONCLUSIONS

In this paper I have shown how the kinematic wavefield attributes of the CRS stack can be utilized for a minimum-aperture Kirchhoff migration. From the attribute α the slope of events in the CRS-stacked section can be computed. This allows to center the migration aperture around the stationary point where the migration operator is tangent to an actual reflection event. The minimum migration aperture (coinciding with the radius of the PFZ) is computed independently for all points in the migration target zone from the CRS attributes. This approach leads to much smaller apertures compared to aperture sizes that must be chosen for conventional Kirchhoff migration. Since the stationary points and the aperture sizes for prestack migration are extrapolated from the values found in the zero-offset case, events occurring only at higher offsets cannot be imaged correctly with this implementation of minimum-aperture prestack migration. Advantages of using minimum apertures are a speed-up of the migration process especially in the prestack case, the avoidance of operator aliasing, and also amplitudes after migration are expected to benefit from the decreased aperture sizes, especially for data with low S/N ratio. To further speed up the migration, the presented method could be combined with the efficient traveltime interpolation and computation of true-amplitude weights presented by Vanelle et al. (2004). By using the attributes of the 3D CRS stack, the presented technique for minimum-aperture Kirchhoff migration can be extended to 3D migration.

ACKNOWLEDGMENTS

This work was kindly supported by the sponsors of the *Wave Inversion Technology (WIT) Consortium*, Karlsruhe, Germany. I thank the energy resource company for providing the real data set.

REFERENCES

Duveneck, E. (2004). Velocity model estimation with data-derived wavefront attributes. *Geophysics*, 69(1):265–274.

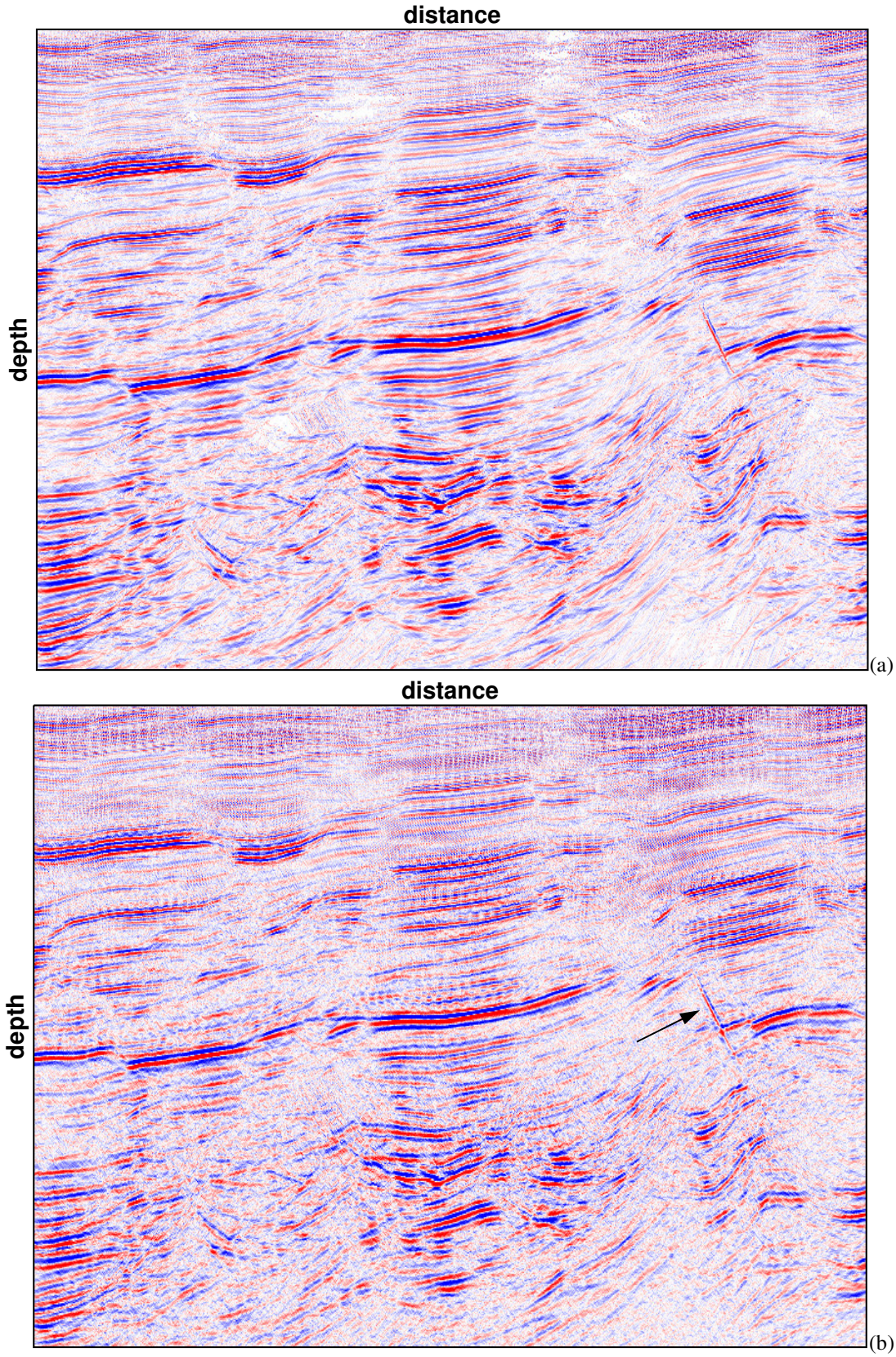

Figure 13: Poststack Kirchhoff migration with minimum aperture determined from CRS attributes (a) and conventional Kirchhoff migration (b) with an aperture increasing linearly with depth.

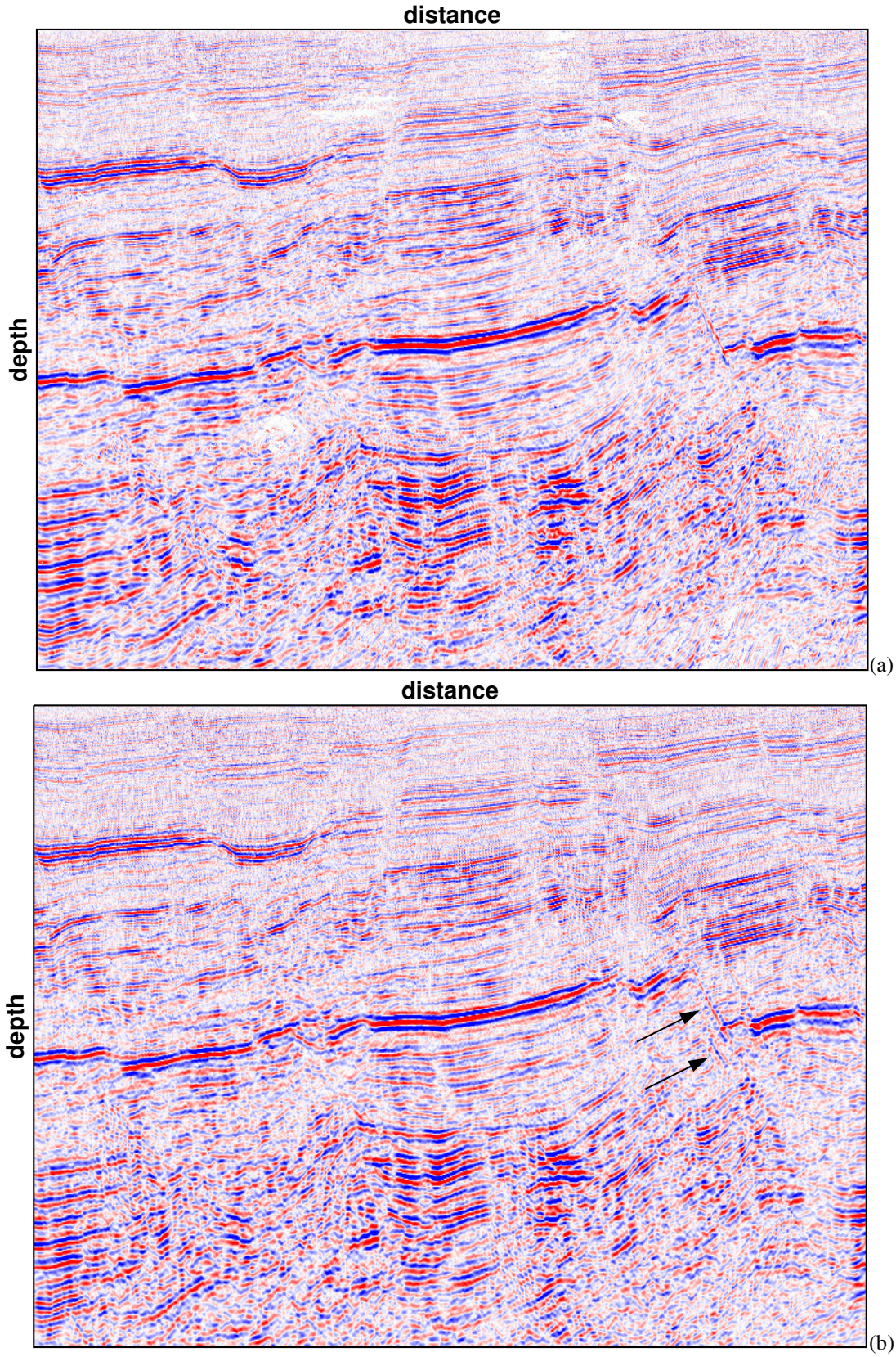

Figure 14: Prestack Kirchhoff migration with minimum aperture determined from CRS attributes (a) and conventional Kirchhoff migration (b) with an aperture increasing linearly with depth. Stack over offsets.

Hanitzsch, C. (1997). Comparison of weights in prestack amplitude-preserving Kirchhoff depth migration. *Geophysics*, 62:1812–1816.

Höcht, G., de Bazelaire, E., Majer, P., and Hubral, P. (1999). Seismics and optics: hyperbolae and curvatures. 42(3,4):261–281.

Jäger, R., Mann, J., Höcht, G., and Hubral, P. (2001). Common-Reflection-Surface stack: Image and attributes. *Geophysics*, 66:97–109.

Koglin, I. and Ewig, E. (2003). Residual static correction by means of CRS attributes. In *Expanded Abstracts*. 73rd Ann. Internat. Mtg., Soc. Expl. Geophys. Session SP 1.4.

Mann, J. (2002). *Extensions and Applications of the Common-Reflection-Surface Stack Method*. Logos Verlag, Berlin.

Müller, T. (1999). *The Common Reflection Surface Stack Method – Seismic imaging without explicit knowledge of the velocity model*. Der Andere Verlag, Bad Iburg.

Pruessmann, J., Coman, R., Endres, H., and Trappe, H. (2004). Improved imaging and AVO analysis of a shallow gas reservoir by CRS. *The Leading Edge*, 23(9):915–918.

Schleicher, J., Hubral, P., Tygel, M., and Jaya, M. (1997). Minimum apertures and Fresnel zones in migration and demigration. *Geophysics*, 62:183–194.

Vanelle, C., Spinner, M., Hertweck, T., Jäger, C., and Gajewski, D. (2004). Traveltime-based true-amplitude migration. *WIT report*.

Vieth, K.-U. (2001). *Kinematic wavefield attributes in seismic imaging*. PhD thesis, University of Karlsruhe.